Electrochimica Acta 368 (2021) 137594

Contents lists available at ScienceDirect

Electrochimica Acta

journal homepage: www.elsevier.com/locate/electacta

Effects of organic additives on the impurity and grain structure of electrodeposited cobalt

Y. Hu[a], S. Deb[b], D. Li[c], Q. Huang[a,*]

[a] Department of Chemical and Biological Engineering, University of Alabama, Tuscaloosa, AL 35487, United States
[b] Department of Chemistry and Biochemistry, University of Alabama, Tuscaloosa, AL 35487, United States
[c] Pacific Northwest National Laboratory, Richland, WA 99354, United States

ARTICLE INFO

Article history:
Received 21 September 2020
Revised 10 November 2020
Accepted 30 November 2020
Available online 9 December 2020

Keywords:
Cobalt electrodeposition
Interconnects
Impurity
Grain structure
Organic additive

ABSTRACT

Co films were electrodeposited with different additives including dimethylglyoxime, sodium chloride, and mercapto-propanesulfonate (MPS). A systematic study was conducted using scanning electron microscope, four-point probe, secondary ion mass spectrum, and X-ray diffraction to understand the effects of such additives on the morphology, resistivity, impurity incorporation, and grain structure of film, as well as how thermal annealing influences these attributes. The addition of MPS into the electrolyte was found to significantly increase the S incorporation level and decrease the grain size, both contributing to a higher sheet resistance of film. Transmission electron microscope with energy dispersive X-ray spectroscopy and local electrode atom probe tomography were used to determine the distribution of different impurity elements. A pronounced grain structure change from columnar grains to pseudo-spherical grains was observed upon the addition of MPS in electrolyte or the incorporation of S in film. In addition to the precipitation of sporadic S-rich clusters, S and C were also found to segregate at the grain boundaries in annealed Co films, both of which are believed to correlate to the grain growth and a significant resistance drop upon annealing.

Introduction

Copper (Cu) has been used as the conducting metal in back end of the line (BEOL) wiring for many CMOS technology generations [1]. Electrodeposited Cu was selected not only for the defect-free superconformal filling enabled by organic additives [2] but also because of the self-annealing phenomenon [3], where the as deposited fine-grained Cu undergoes abnormal grain growth at room temperature resulting in a much improved resistivity and reliability. However, as the BEOL critical dimensions decrease to the mean free path of Cu or below, the resistivity of Cu in fine features increases exponentially [4], posing significant challenges on the further scaling of interconnects and demanding alternative materials [5]. Among them, cobalt (Co) has been proposed, explored and, recently, adopted as one of the front runners to replace copper in the finest metal levels [6]. The electron mean free path in Co is much shorter than Cu, allowing further scaling. On the other hand, a higher melting point of Co (than Cu) provides advantages as it decreases diffusion and electromigration.

Damascene Cu plating processes have been well established in the industry. Not only have the different roles of organic additives in such processes been extensively investigated [7], but also much effort has been made to understand the recrystallization and the effect of impurity on such recrystallization of the electrodeposited Cu films [8–10]. As discussed above, the so-called “self-annealing”, or room temperature grain growth, was typically observed for electrodeposited Cu films with a fine grain size and minimum amount of impurity elements [11]. The latter is dependent on the deposition conditions and the organic additives used [12]. Due to the local deviation of the additive concentration or distribution inside the narrow trenches to be filled, the impurity incorporation behavior in small structures can be significantly different from that of a film, and the annealing process in BEOL fabrication is therefore typically carried out at an elevated temperature to facilitate, expedite and stabilize the grain growth.

While the effects of additive, annealing, and impurity incorporation on electrodeposited Cu have been well established [13–15], very few reports are available on Co. Kelly et al. [16] reported a comprehensive study about Co film properties with different deposition methods (physical vapor deposition, chemical vapor deposition, and electrodeposition) and annealing treatment. The resistivity of Co films with different deposition methods was measured

* Corresponding author.
E-mail address: qhuang@eng.ua.edu (Q. Huang).

https://doi.org/10.1016/j.electacta.2020.137594
0013-4686/

and compared. Moreover, they found that the impurity level of Co films was related to deposition methods, electrolyte composition, and annealing process. Doubina et al. recently conducted a systematic study on the thermal annealing effect on the grain structure of plated Co films and lines, where grain coarsening was observed at around 300 to 350 °C [17]. In our previous work [18–20], additives with a pair of conjugated oxime groups such as dimethylglyoxime (DMG) display strong suppression effects on Co deposition and a suppression breakdown occurred upon the reduction of adsorbed Co^{2+}-dioxime chelates. Superconformal filling using such additives has also been demonstrated and results will be published separately. In this paper, the effects of DMG additive and annealing process on the impurity incorporation, film sheet resistance, and grain structure of electrodeposited Co are reported. The impacts of two co-additives, sodium chloride (NaCl) and sodium 3-mercapto-1-propanesulfonate (MPS), are also investigated here as the source of Cl and S impurities, respectively.

Experimental

A homemade electrochemical cell with an electrolyte bridge to separate the catholyte and anolyte was used in this study. The counter electrode was a Co rod with a purity at least 99.9% and a surface area much larger than that of the cathode. Si coupons (2 cm by 2 cm squares, or 4 cm^2) were cleaved from a 3-inch blanket wafer with Co (30 nm, PVD) seed layer on Ta (5 nm, PVD) adhesion layer, and were used as cathodes. The Si coupon was mounted on a holder rotating in the same way as a rotating disk electrode. The electrical connection was made through a front pin contact to the Co seed. All Co films were deposited at −15 mA/cm^2 and 400 rpm for 400 s, corresponding to a thickness between 640 and 910 nm depending on the Faraday efficiency. This current density was selected as it is used in BEOL metallization. The selection is also based on our previous studies, where the suppression by DMG has broken down and impurity incorporation is expected to occur [20]. After electrodeposition, all films were thoroughly rinsed in deionized (DI) water and then blow-dried using compressed air before analysis.

The Co makeup solution for deposition was the same as our previous studies, containing 0.3 M $CoSO_4$, 0.4 M H_3BO_3, and 0.1 g/L sodium dodecyl sulfate (SDS). The pH of Co solution was adjusted to 4.0 with H_2SO_4. Concentrated DMG solution (23,000 ppm), concentrated MPS solution (17,800 ppm), and concentrated NaCl solution (3550 ppm of Cl) were prepared by dissolving the corresponding chemicals in water. Calculated amounts of the concentrated additive solutions were then added into the Co makeup solution to introduce 100 ppm of each additive. All salts and organic additives were at least ACS grade and used as received. DI water with a resistivity of 18.2 MOhm-cm was used in all studies.

An Autolab 302 N potentiostat was used for all electrochemical studies. A home-built vacuum annealing system was used to anneal all Co films at 300 °C for overall 20 h. The annealed Co films were cooled down to room temperature before unloading and were kept in N_2 atmosphere in between annealing to minimize oxidation. A four-point probe setup was used to measure the film sheet resistance, a ratio between resistivity to the film thickness. A Bruker D8 powder X-ray diffractometer (XRD) with Co Kα source (wavelength = 1.79 Å) was used to perform film crystallographic analysis. The D8 powder diffractometer is equipped with a 2-dimensional x-ray detector, which collects the x-ray signal within a θ range from θ-α to θ+α. The range α is determined by the size of the detector and its distance from the specimen. During the data acquisition, the x-ray tube and detector are both fixed at same positions, θ1, θ2, or θ3, resulting in the collection of multiple segments of diffraction pattern. The neighboring segments slightly overlap so that a complete diffraction pattern is obtained by merging them together. The 2θ resolution used in data acquisition is 0.005°. A JEOL 7000 scanning electron microscope (SEM) was used to characterize the morphology of electrodeposited Co films, operated at 30 kV. Time-of-flight secondary ion mass spectroscopy (ToF-SIMS) equipped with a Bi cluster liquid metal ion source was used to obtain the depth profiles of various elements in the electrodeposited Co films. Since the electrodeposited Co are dense films without porosity or density change, the SIMS signal of a same element between different Co films can be used as a direct comparison of the concentration of impurity. However, a comparison between different elements would be inaccurate due to the yield difference for different elements. A FEI Quanta 3D Dual Beam (FIB) with a 30 kV gallium ion beam was used to prepare samples for transmission electron microscope (TEM) and local electrode atom probe (LEAP) tomography. Cross-sectional grain structure observation with elemental analysis was carried out using FEI TITAN TEM with a Bruker EDAX energy dispersive spectroscopy (EDS) detector. A Cameca LEAP 5000 XS was used to analyze the specimens prepared with FIB. The base temperature was maintained at 30 K during analysis, and the specimens were analyzed with a laser power of 0.05 nJ. Atoms were ionized using high-voltage pulses at a frequency of 200 kHz.

Results and discussion

The effects of additives on the morphology of electrodeposited Co were first characterized using SEM and Fig. 1 shows the top-down images. The Co film prepared in additive-free solution shows large and flake-shaped Co grains with sharp ridges, which is consistent with the literature [21]. Moreover, no significant changes in the shape or size of grains are observed after vacuum annealing at 300 °C for up to 20 h. This also confirms that no significant oxide has formed during or between annealing studies. The film morphology, however, has dramatically changed after the addition of 100 ppm DMG. The flake-shaped Co grains become smaller and less frequent, and more irregular Co grains are observed. Based on our previous studies, DMG suppresses Co deposition and catalyzes hydrogen evolution reaction. The continuous formation and adsorption of Co^{2+}-DMG complex may have prevented the growth of large Co nuclei. Adding 100 ppm NaCl into the solution further changes the shape of Co grains, that is, the flake shaped grains become even more sparse and the majority of grains are more spherical. This seems to suggest that the film deposition is dominated by the effect of DMG and this effect might be strengthened by the presence of chloride anion. A fourth case was studied with 100 ppm MPS added into the solution with DMG. Different from the chloride ion, the addition of MPS dramatically changed the film morphology. The size of Co particles further decreases and worm-shaped morphology features appear. It is noted here that the SEM images are at different magnifications for different films and that the worm-shaped features observed here are indeed much smaller than the ridged flake shaped particles in the additive free case. Thiol terminated molecules are known to bond with transition metal surfaces such as Co and form a mono layer [22]. Our recent work shows that the adsorption and desorption of MPS, or a Co-MPS complex, on deposited Co can sometimes be manifested as a spontaneous electrochemical oscillation at certain conditions [23]. The change of film morphology observed here seems to be consistent with the presence of a second adsorbate upon the addition of MPS. If a competitive adsorption between two adsorbates (Co-MPS complex and Co^{2+}-DMG complex) occurs, depending on the interaction of the two, the change of the surface coverages would be expected to have an impact on the nucleation, growth, and therefore morphology of films. On the other hand, the annealing process completely changes the surface morphology, where the worm-shaped features disappear and a dense compact film with small

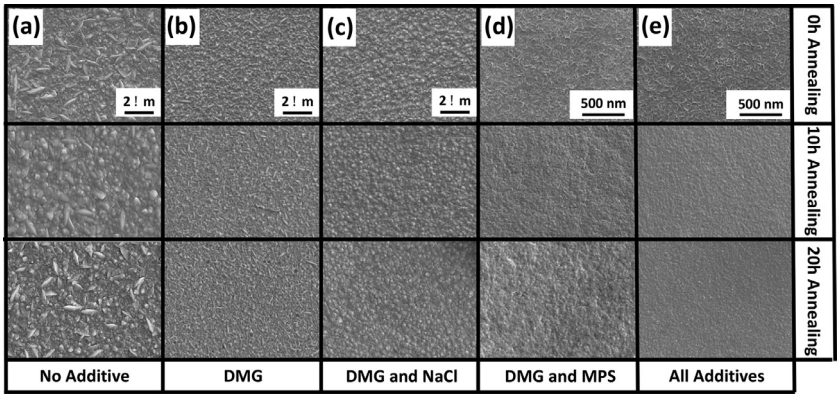

Fig. 1. Top-down SEM images of electrodeposited Co films from solution containing (a) no additive; (b) 100 ppm DMG; (c) 100 ppm DMG and NaCl; (d) 100 ppm DMG and MPS and (e) 100 ppm DMG, NaCl, and MPS before and after annealing.

spherical grains was obtained. When all three additives (DMG, Cl, MPS) are present in the solution, the surface morphology is similar to the case with only two additives, DMG and MPS, consistent with the above discussion on the stronger effects from DMG and MPS than chloride ion.

The effects of additive on impurity incorporation in Co films were studied using SIMS. The elemental depth profiles are shown in Fig. 2. The profiling runs from the top surface of Co to the silicon (Si) substrate. The depth of the raster crater was determined with an AFM stylus. A sharp increase of Si signal upon the emerge of substrate is used as the end point of analysis and to estimate the thickness of Co film. In addition, the volatile CN species is used in SIMS to represent the concentration of N. Fig. 2(a) and (b) show the depth profiles of Co films deposited without additives and with 100 ppm DMG, respectively. The SIMS signals of all impurity elements are much higher at the film surface, i.e. the beginning of analysis, because of the surface oxide as well as the matrix effect on the signal yield. A stable region is observed under this surface layer for all cases, reflecting a steady state deposition process. The film thickness decreases from 780 nm to 640 nm upon the addition of DMG, where the Co deposition is suppressed. The presence of DMG also enhances the hydrogen evolution reaction [24,25], further decreasing the current efficiency and film thickness in galvanostatic deposition. The comparison between the two films shows that the amount of N, measured as the count of CN species, dramatically increases for 20 times, from 50 to 1000 after DMG is added. At the same time, the counts of C and S both increase for about 7 times, from 15 to 100. Since DMG is the only N source in the electrolyte, the significant increase of CN species agrees with our previous work [20], where the suppression effect of dioxime on Co deposition was concluded to result from a Co^{2+}-dioxime complex formed through a pair of conjugated N-atoms in dioxime. The complex molecule adsorbs on electrode surface inhibiting Co deposition, but breaks down and gets incorporated into film at a sufficiently negative potential or a cathodic current. Interestingly, the increase of C signal is much less pronounced than N. Because the SIMS signal was not calibrated using a standard, it is unclear if this difference results from the different yields of element or a lower incorporation of C. The latter, if true, may suggest that the C–N bond in DMG breaks frequently upon the DMG incorporation.

The SIMS results here also show that the formation and incorporation of this Co^{2+}-DMG adsorbate facilitates the incorporation of sulfur, an element not present in DMG. This suggests a co-incorporation from the inorganic sulfate or the surfactant dodecyl sulfate. However, neither anion shows strong affinity with electrode surface, particularly at a negatively biased surface, resulting in very low S incorporation. Such co-incorporation is also observed for chloride, probably from the inevitable contamination from laboratory ambient or impurities in chemicals, but to a much lower degree and with a much lower concentration.

Fig. 2(c) shows the depth profile of Co film deposited with 100 ppm DMG and 100 ppm MPS. A comparison with Fig. 2(a) shows a significant increase of S concentration from 100 to 10,000, suggesting that MPS dominates the S incorporation in the Co film. This is not uncommon as the thiol group has a strong affinity with metal and such a significant S incorporation has been widely observed in Cu deposition in presence of MPS [26]. More interestingly, the concentration of CN decreases 3 folds, from 1000 to 300, while other elements such as C, O, and Cl all remained about the same**,** indicative of a lower incorporation rate of DMG in the presence of MPS. As discussed above in Fig. 1, it is believed that both Co-MPS complex and Co^{2+}-DMG complex are adsorbed on electrode surface and suppress Co deposition. Therefore, this result not only demonstrates a competitive adsorption between the Co^{2+}-DMG and Co-MPS complexes, but also confirms a direct correlation between impurity incorporation with surface adsorbates. Moreover, the thickness of these two films are nearly the same, which means the addition of MPS on top of DMG does not further change the current efficiency of Co deposition. When all three additives are present in the solution, shown in Fig. 2(d) and similar to Fig. 2(c), only S and CN incorporation increase compared with Fig. 2(a). Surprisingly though, the concentration of Cl in film maintains at a similar level despite the addition of NaCl in electrolyte. The addition of Cl on top of DMG and MPS results in a decrease in S incorporation. It also results in an increase in current efficiency at the deposition condition used as the film thickness increases from about 640 nm to 910 nm. The mechanism is not clear and no significant impact was observed in film morphology. Fig. 2(e) shows the impurity profile of the same sample in Fig. 2(d), deposited with all additives but after 300 °C vacuum annealing for 20 h. All impurities remain nearly the same except for CN concentration, which decreases for about 50% upon the annealing. It is not shown here, but the amount of H in Co film decreases significantly upon annealing as well. Both H and N can form volatile species themselves and do not form strong ionic bonds with Co metal. Such attributes are different from other impurity elements such as C, O, Cl, S, and are believed to cause the decrease of their concentrations upon annealing.

It is well known that the impurities in copper films have a strong impact on grain coarsening upon annealing, typically characterized as a decrease of sheet resistance along annealing. A similar study was carried out and Fig. 3(a) illustrates the sheet resistance change of five Co films deposited with different additives along a course of 20-h annealing at 300 °C. Before annealing, it is

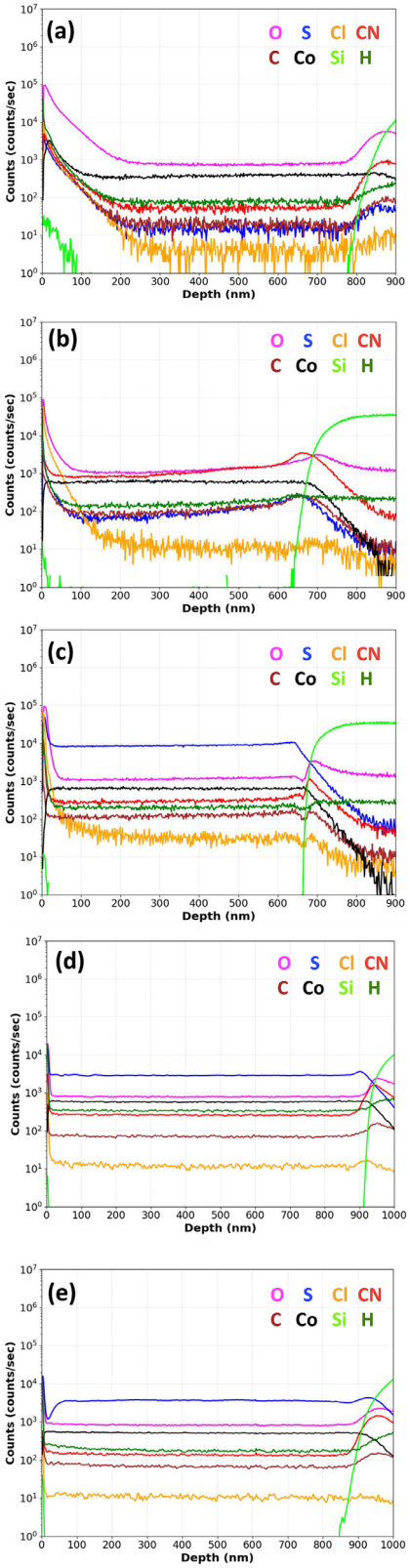

Fig. 2. SIMS elemental depth profiles of electrodeposited Co films from solution containing (a) non-additive before annealing; (b) 100 ppm DMG before annealing; (c) 100 ppm DMG and MPS before annealing; (d) 100 ppm DMG, NaCl, and MPS before annealing and (e) 100 ppm DMG, NaCl, and MPS after 20 h annealing.

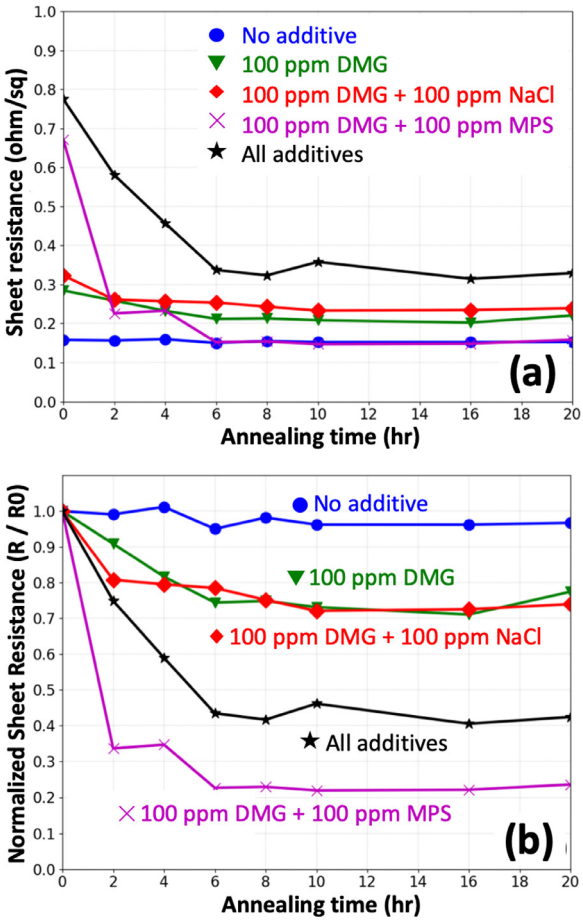

Fig. 3. (a) Sheet resistance change with different additives and annealing conditions as indicated and (b) Normalized Sheet resistance change with different additives and annealing conditions as indicated.

evident that the higher sheet resistance seems to correlate with higher impurity levels in the film. The Co film deposited without additive shows the lowest sheet resistance at around 0.158 Ω/sq. This sheet resistance approximately doubles with the presence of DMG in electrolyte, and almost quintuples upon the addition of MPS on top of DMG. Moreover, the addition of Cl has shown very little increase in the sheet resistance, apparently consistent with the observation in morphology, where DMG and MPS also show the most predominant effects over Cl. It is worth noting here that the film thickness is not a constant as the current efficiency changes. But the change in film thickness estimated from SIMS profiles is much less pronounced than the sheet resistance. For example, the film thickness decreases for about 20% from additive free case in Fig. 2(a) to the DMG with MPS case in Fig. 2(c), but the sheet resistance increases for about 400%. In conjunction with the SIMS results, it can be seen that the addition of MPS or the incorporation of S seems to contribute to such a huge increase in sheet resistance. The sheet resistance is further normalized with the as-deposit resistance value (R0) and is presented in Fig. 3(b), where the resistance decreases along annealing and stabilizes after about 6 hours. The sheet resistance of S-containing Co films, namely the films deposited with MPS, drastically drops up to 78% after 6 h annealing. The resistance evolution for Co films deposited with additives but without MPS, that is, films with much lower S-incorporation, stabilizes at about 30%, regardless of the presence of Cl. No significant resistance change is observed for film deposited additive free. Doubina et al. reported [17] that the low resistivity Co film with larger Co grains could be obtained when the film was

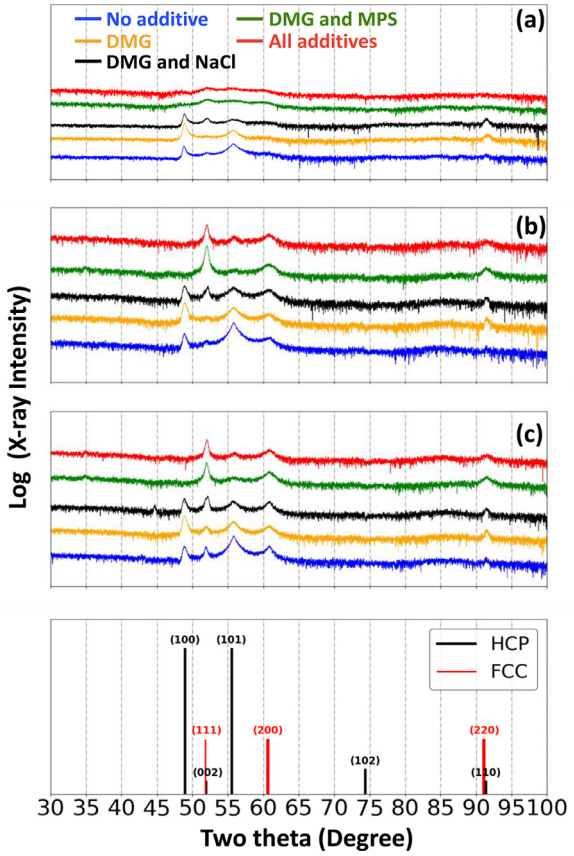

Fig. 4. XRD results of electrodeposited Co films from solution containing different additives with (a) 0 h annealing; (b) 10 h annealing and (c) 20 h annealing.

annealed at 300 °C for 60 min. In our results, the S-containing Co films show the sharp drop of resistance upon 300 °C annealing and similar large grains are observed as shown in Fig. 5(c).

While it is clear that the use of additives in electrolyte leads to the increase of sheet resistance, the effects of these additives differ. Again, the use of MPS and the high S incorporation in film show the strongest impact on sheet resistance, which cause not only the most significant increase of resistance for as deposited films but also the most pronounced decrease of sheet resistance along with annealing. On the other hand, incorporation of C and N from the addition of DMG in electrolyte shows a much less pronounced effect, where the sheet resistance also increases for as deposited films and decreases for annealed films, but both to a lower degree. The change of O and Cl incorporation with different additive combinations are very marginal and no strong effect on the sheet resistance could be determined.

Electrodeposited metal films with fine grains, when annealed, typically experience a change in microstructure, or grain growth, along with the outgassing or redistribution of impurity elements. Such changes often cause a sheet resistance decrease by mitigating the electron scattering at grain boundaries. However, the grain growth behavior or the easiness of grain boundary elimination is highly related to not only the impurity elements but also the grain structures of as deposited films.

The crystallographic structure of films was characterized with X-ray diffraction. Fig. 4(a) shows the diffraction pattern of as-deposited Co films with different additives. The X-ray signal is plotted in the log scale. Both HCP and FCC Co phases are observed in all films. No peak is observed from the single crystal Si substrate with the powder diffractometer used in the study. The Co films deposited without MPS are polycrystalline with a predominant HCP structure, with the sharp peaks at 2θ of 48.8°, 55.5°, 52.5° and 91.2° assigned to Co HCP (100), (101), (002) and (110) orientations, respectively. While two of the peaks at 48.8° and 91.2° are also close to the FCC (111) and FCC (220) reflections, respectively, the FCC (200) peak at 60.6° is broad and weak, suggesting that either the FCC grains are extremely refined or the fraction of FCC phase is extremely minor. This observation holds largely the same regardless of the addition or the absence of DMG and chloride, except for a small shift of the relatively preferred orientation within the HCP phase. The introduction of MPS into the electrolyte significantly changes the crystallinity of Co films. While all the above peaks are also observed, the peaks are much broader and weaker, indicative of much finer grains for both phases. As discussed earlier, these films show a much higher sheet resistance, as well as a much higher sulfur incorporation. Here, the much finer grains are believed to contribute to the higher sheet resistance through grain boundary scattering. Adsorbates such as halides are known to selectively adsorb on certain facets of metal crystals [27]. Such preferences are believed to relate to the change of the preferred crystallographic phases of Co observed here upon the addition of DMG and Cl. However, the addition of MPS seems to cause a ubiquitous peak broadening regardless of the orientation, suggesting that the thiol group in MPS has strong affinity with all Co facets and renders MPS a grain refiner.

Polycrystalline Co films with coarsened grains are obtained upon 300 °C vacuum annealing for 10 h. This grain coarsening effect are more pronounced for the films deposited with MPS, where the grains are refined. As shown in Fig. 4(b), four strong reflections, HCP (002), (101), (110) and FCC (200), emerged after annealing for these films. No significant grain growth is observed in HCP (100) direction. Among the four peaks, HCP (002) seems to be the strongest, indicative of a preferred growth of HCP grains in (002) direction. On the other hand, Co films deposited without MPS show much less pronounced change in the XRD reflections. No notable change other than the emergence of a weak FCC (200) peak at 60.6° is observed. Fig. 4(c) shows the diffraction patterns of the same Co films after 20 h annealing. No further change is observed in crystallinity for Co films deposited with MPS. For the other Co films prepared without MPS, no further change was observed either, except for a sharper HCP (002) peak, suggesting that a crystallographic preference gradually evolves as the annealing continues. This evolution takes longer time and the preference is less prominent than the films prepared with MPS. This is consistent with the fact that the latter have much finer grains, that is, much higher grain boundary energy and easier boundary elimination or grain growth. However, it is known from SIMS results that the films also incorporate different impurity elements, particularly S and, to some extent, N. Impurities can increase film resistivity through electron scattering on these foreign elements. More importantly, depending on the mobility, they may segregate at grain boundaries as grains grow. Such segregated impurity can pin the grain boundary, slowing down the grain growth and resistance drop during annealing. Microscopic composition analysis techniques are needed to further understand the roles that the different impurities may play in the grain structure and resistivity.

Cross sectional TEM in conjunction with EDS was first attempted to characterize the grain structure and impurity distribution for two of annealed films, one deposited with DMG and the other with all three additives. Both films were deposited for 400 s at a same current density of 15 mA/cm^2 and a same rotation rate of 400 rpm. The conditions are similar to films presented in Fig. 1, and the film thicknesses are also consistent, at about 600 nm. Fig. 5(a) shows the dark field cross-sectional TEM micrographs of Co films with 100 ppm DMG after 20 h annealing. Columnar grains across the entire film thickness are observed with lateral grain size of about 100 nm. EDS elemental maps around a grain boundary are

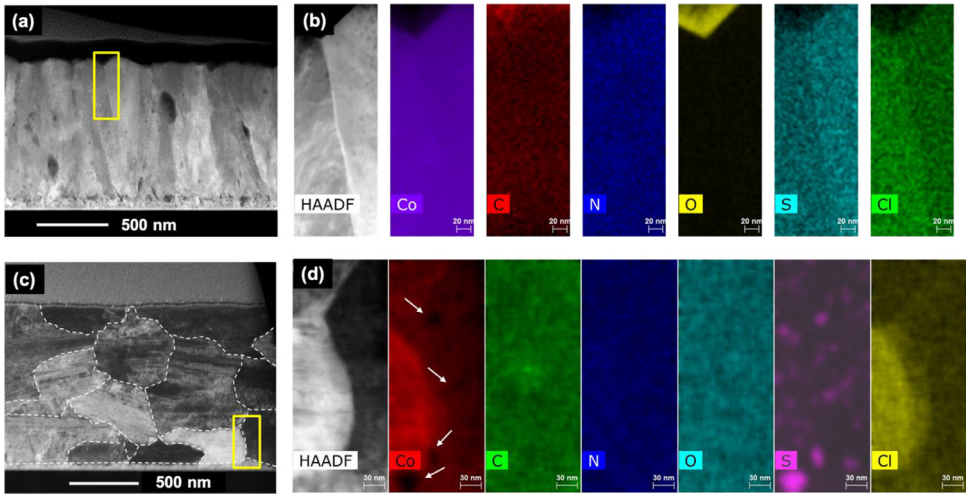

Fig. 5. (a, c) Cross sectional FIB-TEM images and (b, d) EDS elemental maps around a grain boundary of Co films electrodeposited with (a, b) 100 ppm DMG and (c, d) 100 ppm DMG, NaCl, and MPS. Both films were annealed at 300 °C for 20 h annealing. White dashed lines in (c) are used to outline the grains. Yellow boxes in (a, c) are used to outline the location for EDS mapping. (For interpretation of the references to color in this figure legend, the reader is referred to the web version of this article.)

acquired and presented in Fig. 5(b). A slight contrast is observed between the two grains for Co, S, and Cl signals. This is because of the difference in the grain orientation, resulting in different signal intensities. But a uniform distribution of impurities is observed across the grains and grain boundaries. Line scans were also carried out perpendicularly across the grain boundary, but no aggregation of any element could be identified. An organic coating was applied on Co films prior to TEM sample preparation, resulting in the top region rich in carbon and oxygen.

Similar analysis was also carried out for a Co film deposited with all three additives (DMG, MPS, Cl) after 20 h annealing, and the results are shown in Fig. 5(c). As outlined with the white dashed lines, the grain structure dramatically changes as compared with Fig. 5(a). Instead of the columnar grains, randomly distributed, irregular but more spherical, grains with a more uniform size between 200 and 500 nm are obtained. It is known from XRD that the as deposited film has much finer grains. The more spherical grains observed here post anneal suggest a random nucleation of initial grains and an anisotropic grain growth with a more uniform growth rate in all crystal orientations. Elemental maps are also acquired at a boundary between two grains, as indicated with a yellow box in the TEM image, and the results are shown in Fig. 5(d). A clear contrast in signal density was observed between the two grains for Co and Cl, similar to Fig. 5(b). It is worth noting that an intermediate Cl content region seems to be present at the grain boundary, resulting in two apparent boundaries with one on the left of the other. This indicates that the grain boundary in TEM micrograph may not be perfectly perpendicular to the TEM sample lamella and the projected view of the tilted grain results in such halo. Interestingly, whilst an aggregation of impurities at grain boundary could not be determined here, numerous sulfur-rich clusters are clearly observed across the entire field of view. Carbon accumulation occurs as well, albeit to a much less extend, forming one cluster. In addition, a lower cobalt signal is observed in the sulfur clusters (highlighted with white arrows), probably resulting from a combination of different crystal structure and orientation, and a lower cobalt concentration in a cobalt sulfide compound region. Since only one C cluster was observed, multiple regions in the lamella were examined and such observations have been confirmed.

EDS has a typical detection limit of 0.1 wt% [28]. and it can be even poorer for light elements such as the ones of interest in this study. While no impurity segregation at grain boundary is confirmed with TEM-EDS, such segregation cannot be completely ruled out because the impurity concentration at grain boundaries could still be well below the detection limit of EDS. Therefore, local electrode atom probe (LEAP) tomography was carried out to further characterize the distribution of different impurity elements in the annealed Co films. A same film as in Fig. 5(c), deposited with all additives and annealed, was used to ensure high impurity incorporation. Multiple pillars with a footprint diameter of no more than 100 nm were prepared from a TEM lamella to ensure the inclusion of a grain boundary in at least one of the pillars. No stress or charge accumulation was observed and the Co pillars well survived the entire analysis, that is, about 140 nm deep profiling. The entire mass spectrum is provided in Supplementary Material with all peaks assigned to a reasonable species to enable the reconstruction of the 3D pillar. The average concentration of all species other than hydrogen and hydrocarbon are well below 0.1 at% (even much lower in wt%), consistent with Fig. 5, where no distribution other than S-rich clusters could be observed in TEM. Fig. 6 shows the elemental distribution maps projected from an angle where a grain boundary can be clearly identified. As shown in the Co map, clusters rich in S were also observed randomly distributed across the film, consistent with the TEM results. Furthermore, CoO with a *m/z* ratio 75 have been observed as very small clusters randomly distributed across the entire film. However, such clusters were not evident in the oxygen map obtained from TEM EDS, probably due to the much smaller size.

The important result from LEAP analysis is that S and C are found to significantly accumulate at grain boundaries. At the specific view angle in Fig. 6, a "χ" shaped segregation of S and C is observed, where the two impurity elements appear to be complementary to each other in terms of the segregation. In the C map, a "λ" shaped distribution was clearly observed. This "λ" shaped boundary is still observed, but much less pronounced, in S map. In addition, S accumulates along another short grain boundary located upper right to this "λ" shape. Overlapping the two maps not only confirms the same location of the grain boundaries, but also reveals the complete "χ" shape of the segregation.

Three LEAP videos are included in the Supplementary Materials with 360° view of the distribution of S and C in the entire pillar specimen. It can be seen from the videos, particularly the ones revolving around Y and Z axes, that the longer tail of the "λ" shape represents the projection of a curved grain boundary, which intersects the pillar from the top cone surface to the cone base,

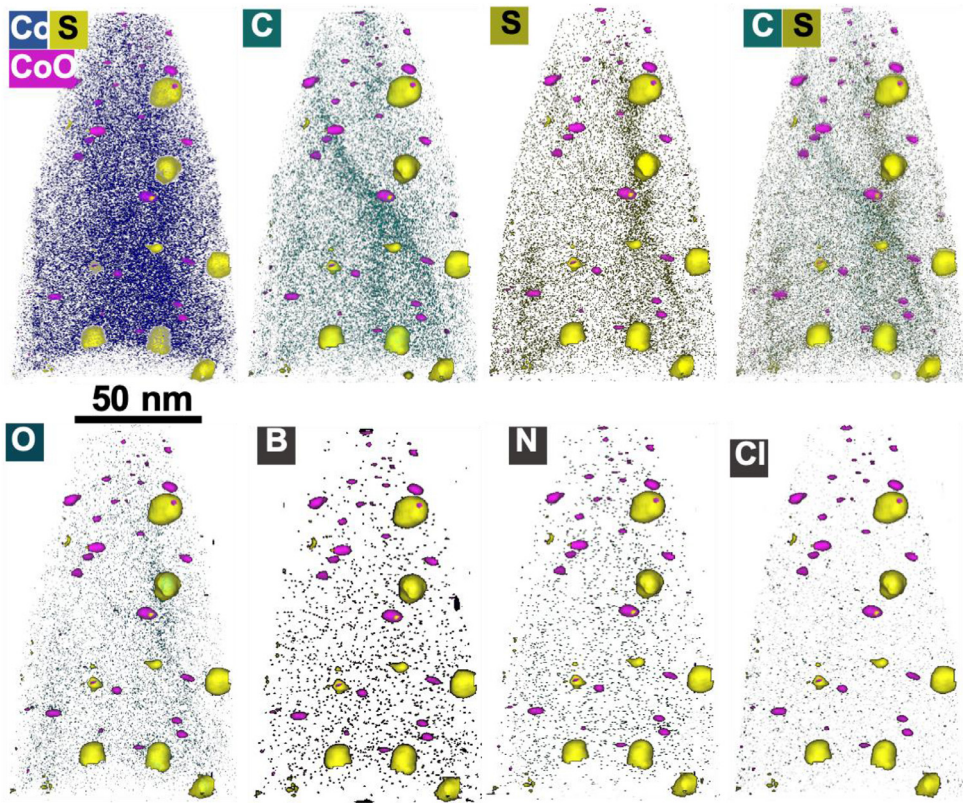

Fig. 6. LEAP tomography elemental mapping and mass spectroscopy results of electrodeposited Co film with 100 ppm DMG, NaCl, and MPS after 20 h annealing.

resulting in a curved trapezoid surface. As discussed in Fig. 4(c), the grains are spherical and grain boundaries are expected to be curved not only in X-Y view plane, but also in Y-Z and X-Z view planes as evidenced in the videos. On the other hand, while the other line of the "χ" shape may also result from a grain boundary, it is less obvious or conclusive. It is worth noting that no morphological patterns were observed on the pillar by SEM that can possibly relate to the observed impurity segregation. While TEM observation was not performed on the same pillar to avoid high energy beam damages, the C and S segregation observed in the 3D animation highly likely corelates to a curved grain boundary. In addition to S and C, some very minor accumulation was observed for O around the cross point of the "χ" shaped boundary. Again, numerous CoO clusters were observed and are believed to be the predominant form of O in the film. This might relate to a stronger electron affinity of O and thus a stronger bond between Co and O, resulting in lower mobility of O. The concentration of other elements such as B, N and Cl, are much lower and no accumulation could be determined.

The effects of the incorporation and movement of impurities have been well studied in the electrodeposited Cu films. It has been reported that a higher annealing temperature not only facilitates the grain boundary annihilation but also promotes impurity mobility, both accelerating the grain growth [29]. Our results here confirm that impurities not only affect the Co grain structure but also redistribute and aggregate in Co films, which is believed to be responsible for the change of sheet resistance.

It is worth mentioning that this Co impurity and microstructure study is based on blanket films, which can be different from fine trenches. Because of the geometry of trench, the growth mode, grain structure, and the impurity incorporation of Co can be different. For example, an additive concentration gradient in the trenches is often needed to achieve the defect free filling. In addition, the current density in the feature is different from the applied current density due to the interaction between additives and the Co surface. Moreover, the filling rate in the trench is typically faster than the deposition on field region. Therefore, as mentioned above, it is very difficult to experimentally mimic the Co deposition in the trenches with a blanket film. Results shown in this study aims to provide a fundamental understanding on the effect of organic additives on the impurity incorporation and grain structure of electrodeposited Co, as well as how the impurities redistribute in relation with grain growth upon annealing.

Conclusion

A systematic study was carried out to understand the effects of additives in electrolyte on the properties of electrodeposited Co films, such as morphology, sheet resistance, grain structure, the incorporation and distribution of impurity elements. The addition of additives, particularly MPS, not only smooths out the film surface, decreases the grain size, and increases the sheet resistance, but also dramatically amplifies the resistance drop upon annealing. SIMS analysis shows that the presence of DMG in electrolyte predominantly introduces N and C impurity into films. On the other hand, the further addition of MPS significantly increases S and decreases N incorporation probably due to a competitive adsorption between the DMG and MPS on electrode surface. XRD confirms that the addition of MPS results in smaller grains in the electrodeposited Co films. While such a refined grain structure contributes to a higher sheet resistance of as deposited Co films, it also eases the grain growth upon annealing resulting in the most significant resistance drop among all the different additive cases studied. Columnar grain structure and pseudo-spherical grains are observed in annealed Co films deposited without and with MPS, respectively. With atom probe tomography, randomly distributed S-rich and CoO clusters in nanometer scale are observed after the an-

nealing of Co films deposited with all additives. More importantly, significant S and C segregation and marginal O segregation at grain boundaries are proved to occur during the annealing, probably correlating to the grain growth. The findings in this study are believed to provide understanding and guidelines for chemistry and process design to fabricate low resistance Co interconnects structures.

Declaration of Competing Interest

The authors declare that they have no known competing financial interests or personal relationships that could have appeared to influence the work reported in this paper.

Credit authorship contribution statement

Y. Hu: Data curation, Investigation, Formal analysis, Writing - original draft, Writing - review & editing. **S. Deb:** Formal analysis, Writing - review & editing. **D. Li:** Formal analysis, Writing - review & editing. **Q. Huang:** Conceptualization, Formal analysis, Writing - original draft, Writing - review & editing.

Acknowledgments

National Science Foundation is acknowledged for support through Grant CMMI-1662332. Preliminary TEM-EDS experiments were supported by the U.S. Department of Energy (DOE), Office of Science (SC), Office of Basic Energy Sciences (BES), Early Career Research program under Award # KC0203020:67037. YH thanks the Graduate Council at The University of Alabama for a fellowship support. Heng-Yong Nie at The University of Western Ontario was acknowledged for SIMS analysis. The Central Analytical Facility at the University of Alabama and the Materials and Manufacturing Research Facility at US Air Force Research Laboratory are acknowledged for the access and training of equipment for characterization.

Supplementary materials

Supplementary material associated with this article can be found, in the online version, at doi:10.1016/j.electacta.2020.137594.

References

[1] P.C. Andricacos, C. Uzoh, J.O. Dukovic, J. Horkans, H. Deligianni, Damascene copper electroplating for chip interconnections, IBM J. Res. Dev. 42 (5) (1998) 567.
[2] T. Moffat, D. Wheeler, W. Huber, D. Josell, Superconformal electrodeposition of copper, Electrochem. Solid-State Lett. 4 (4) (2001) C26.
[3] J. Harper, C. Cabral Jr, P. Andricacos, L. Gignac, I. Noyan, K. Rodbell, C. Hu, Mechanisms for microstructure evolution in electroplated copper thin films near room temperature, J. Appl. Phys. 86 (5) (1999) 2516.
[4] W. Steinhögl, G. Schindler, G. Steinlesberger, M. Engelhardt, Size-dependent resistivity of metallic wires in the mesoscopic range, Phys. Rev. B 66 (7) (2002) 075414.
[5] D. Gall, Electron mean free path in elemental metals, J. Appl. Phys. 119 (8) (2016) 085101.
[6] F.W. Mont, X. Zhang, W. Wang, J.J. Kelly, T.E. Standaert, R. Quon, E.T. Ryan, Cobalt interconnect on same copper barrier process integration at the 7nm node, in: Proceedings of the 2017 IEEE International Interconnect Technology Conference (IITC), 1, 2017.
[7] T.P. Moffat, D. Wheeler, S.-K. Kim, D. Josell, Curvature enhanced adsorbate coverage model for electrodeposition, J. Electrochem. Soc. 153 (2) (2006) C127.
[8] J. Kelly, T. Nogami, O. Van der Straten, J. Demarest, J. Li, C. Penny, T. Vo, C. Parks, P. DeHaven, C.-K. Hu, Electrolyte additive chemistry and feature size-dependent impurity incorporation for Cu interconnects, J. Electrochem. Soc. 159 (10) (2012) D563.
[9] Q. Huang, A. Avekians, S. Ahmed, C. Parks, B. Baker-O'Neal, S. Kitayaporn, A. Sahin, Y. Sun, T. Cheng, Impurities in the electroplated sub-50nm Cu lines: the effects of the plating additives, J. Electrochem. Soc. 161 (9) (2014) D388.
[10] M. Stangl, M. Lipták, J. Acker, V. Hoffmann, S. Baunack, K. Wetzig, Influence of incorporated non-metallic impurities on electromigration in copper damascene interconnect lines, Thin Solid Films 517 (8) (2009) 2687.
[11] S. Lagrange, S. Brongersma, M. Judelewicz, A. Saerens, I. Vervoort, E. Richard, R. Palmans, K. Maex, Self-annealing characterization of electroplated copper films, Microelectron. Eng. 50 (1–4) (2000) 449.
[12] M. Stangl, M. Liptak, A. Fletcher, J. Acker, J. Thomas, H. Wendrock, S. Oswald, K. Wetzig, Influence of initial microstructure and impurities on Cu room-temperature recrystallization (self-annealing), Microelectron. Eng. 85 (3) (2008) 534.
[13] K. Barmak, A. Gungor, C. Cabral Jr, J. Harper, Annealing behavior of Cu and dilute Cu-alloy films: precipitation, grain growth, and resistivity, J. Appl. Phys. 94 (3) (2003) 1605.
[14] L. Bonou, M. Eyraud, R. Denoyel, Y. Massiani, Influence of additives on Cu electrodeposition mechanisms in acid solution: direct current study supported by non-electrochemical measurements, Electrochim. Acta 47 (26) (2002) 4139.
[15] C.-K. Hu, L. Gignac, B. Baker, E. Liniger, R. Yu, P. Flaitz, Impact of Cu microstructure on electromigration reliability, in: Proceedings of International Interconnect Technology Conference, 93, IEEE, 2007 2007.
[16] J. Kelly, V. Kamineni, X. Lin, A. Pacquette, M. Hopstaken, Y. Liang, H. Amanapu, B. Peethala, L. Jiang, J. Demarest, Annealing and impurity effects in co thin films for MOL contact and BEOL metallization, J. Electrochem. Soc. 166 (1) (2019) D3100.
[17] N.V. Doubina, T.A. Spurlin, E.C. Opocensky, J.D. Reid, The effect of thermal annealing on cobalt film properties and grain structure, MRS Adv. 5 (37-38) (2020) 1919.
[18] Q. Huang, T. Lyons, W. Sides, Electrodeposition of cobalt for interconnect application: effect of dimethylglyoxime, J. Electrochem. Soc. 163 (13) (2016) D715.
[19] Y. Hu, Q. Huang, Effects of dimethylglyoxime and cyclohexane dioxime on the electrochemical nucleation and growth of cobalt, J. Electrochem. Soc. 166 (1) (2019) D3175.
[20] T. Lyons, Q. Huang, Effects of cyclohexane-monoxime and dioxime on the electrodeposition of cobalt, Electrochim. Acta 245 (2017) 309.
[21] N. Pradhan, P. Singh, B. Tripathy, S. Das, Electrowinning of cobalt from acidic sulphate solutions—effect of chloride ion, Miner. Eng. 14 (7) (2001) 775.
[22] A. Caruso, L. Wang, S. Jaswal, E.Y. Tsymbal, P.A. Dowben, The interface electronic structure of thiol terminated molecules on cobalt and gold surfaces, J. Mater. Sci. 41 (19) (2006) 6198.
[23] Q.H. Yang Hu, Oscillatory behavior in cobalt electrodeposition with 3-mercapto-1-propanesulfonate, J. Phys. Chem. C 124 (39) (2020) 21608.
[24] P.-A. Jacques, V. Artero, J. Pécaut, M. Fontecave, Cobalt and nickel diimine–dioxime complexes as molecular electrocatalysts for hydrogen evolution with low overvoltages, Proc. Natl. Acad. Sci. 106 (49) (2009) 20627.
[25] C.N. Valdez, J.L. Dempsey, B.S. Brunschwig, J.R. Winkler, H.B. Gray, Catalytic hydrogen evolution from a covalently linked dicobaloxime, Proc. Natl. Acad. Sci. 109 (39) (2012) 15589.
[26] H. Demers, U. Emekli, E. Lifshin, A. West, Characterization of electrodeposited copper films with time-of-flight SIMS, Microsc. Microanal. 15 (S2) (2009) 492.
[27] S. Ghosh, L. Manna, The many "facets" of halide ions in the chemistry of colloidal inorganic nanocrystals, Chem. Rev. 118 (16) (2018) 7804.
[28] J.I. Goldstein, D.E. Newbury, J.R. Michael, N.W. Ritchie, J.H.J. Scott, D.C. Joy, Scanning Electron Microscopy and X-ray Microanalysis, Springer, 2017.
[29] S. Brongersma, E. Kerr, I. Vervoort, A. Saerens, K. Maex, Grain growth, stress, and impurities in electroplated copper, J. Mater. Res. 17 (3) (2002) 582.